



This is a repository copy of *Computational optical sectioning via near-field multi-slice ptychography*.

White Rose Research Online URL for this paper:

<https://eprints.whiterose.ac.uk/217298/>

Version: Published Version

Article:

Hu, Z. orcid.org/0000-0001-7306-883X, Zhang, Y. and Maiden, A. orcid.org/0000-0002-8192-8235 (2024) Computational optical sectioning via near-field multi-slice ptychography. *Optics Letters*, 49 (17). pp. 4839-4842. ISSN 0146-9592

<https://doi.org/10.1364/ol.529190>

Reuse

This article is distributed under the terms of the Creative Commons Attribution (CC BY) licence. This licence allows you to distribute, remix, tweak, and build upon the work, even commercially, as long as you credit the authors for the original work. More information and the full terms of the licence here:

<https://creativecommons.org/licenses/>

Takedown

If you consider content in White Rose Research Online to be in breach of UK law, please notify us by emailing eprints@whiterose.ac.uk including the URL of the record and the reason for the withdrawal request.



eprints@whiterose.ac.uk
<https://eprints.whiterose.ac.uk/>

Computational optical sectioning via near-field multi-slice ptychography

ZIYANG HU,^{1,*}  YIQIAN ZHANG,¹ AND ANDREW MAIDEN^{1,2} 

¹EEE Department, The University of Sheffield, Sheffield, S1 3JD, UK

²Diamond Light Source, Diamond House, Oxfordshire, OX11 0DE, UK

*zhu9@sheffield.ac.uk

Received 16 May 2024; revised 24 July 2024; accepted 30 July 2024; posted 31 July 2024; published 21 August 2024

We introduce a method for the computational sectioning of optically thick samples based on a combination of near-field and multi-slice ptychography. The method enables a large field-of-view 3D phase imaging of samples that is an order of magnitude thicker than the depth of field of bright-field microscopy. An axial resolution for these thick samples is maintained in the presence of multiple scattering, revealing a complex structure beyond the depth of the field limit. In this Letter, we describe the new, to the best of our knowledge, approach and demonstrate its effectiveness using a range of samples with diverse thicknesses and optical properties.

Published by Optica Publishing Group under the terms of the [Creative Commons Attribution 4.0 License](https://creativecommons.org/licenses/by/4.0/). Further distribution of this work must maintain attribution to the author(s) and the published article's title, journal citation, and DOI.

<https://doi.org/10.1364/OL.529190>

Introduction. As a tool for optical microscopy, ptychography has been implemented in myriad forms, including microscope add-ons, stand-alone systems and as a system-on-chip [1–3]. Unlike x ray and electron ptychography, the key advantages of the method at optical wavelengths comes not from its lens-free operation but from the contrast enhancement offered by phase imaging and the ability, especially of Fourier ptychography, to extend an optical system's space–bandwidth product. In this Letter, we combine these benefits with one of ptychography's other facets: accommodating multiple scatter and diffraction when imaging optically thick samples, via the multi-slice method [4]. The multi-slice, or beam propagation, method models an optically thick sample as a series of slices and approximates the passage of the beam through these slices via a series of multiplications (current beam wavefront times current slice) and propagations (free-space propagation from the current slice to the next). Combining this multi-slice model with ptychographic phase retrieval has proven a successful means of extending the depth of field (DoF) [5–10], while implementation as a microscope add-on, either in Fourier or conventional sample-scanning geometries, has enabled computational optical sectioning, where the axial or z resolution of the slicing reduces to the micron scale [5,11]. The approach we propose here continues this theme, enhancing a standard microscope through a combination of multi-slice and near-field ptychography (where interference

patterns are recorded at Fresnel numbers $\gg 1$) [12,13] to realize extended field-of-view computational optical sectioning, free from the effects of multiple scattering and diffraction. Unlike previous multi-slice implementations, our method combines the following benefits: a fixed optical path, allowing the recovered illumination wavefront to factor in beam inhomogeneities and coherent artifacts so that they do not affect the reconstruction; a large and extendable field of view, covered using a relatively small number of diffraction patterns; and a revised reconstruction algorithm that offers robust, quick convergence. We demonstrate the method's capability to image phase at a diffraction-limited resolution of around 1 μm for samples ranging in thickness from 40 to 140 μm .

Experiment configuration. The optical arrangement of our multi-slice microscope is shown in Fig. 1(a). A fiber-coupled 675 nm diode laser first passes through a ground glass diffuser and a square aperture that limits the extent of the beam. The resulting structured wavefront is projected onto the sample through a condenser lens ($\text{NA} = 0.4$). The fiber tip and back focal plane of the condenser are conjugated, so that the wavefront between the condenser and objective lenses is collimated. The sample is axially offset by 25 μm from the image plane of a standard compound microscope comprising a 20 \times , $\text{NA} = 0.5$ objective and $f = 180$ mm tube lens. This results in near-field diffraction patterns imaged onto the detector, a PCO edge 4.2 with a pixel pitch of 6.5 μm . The diffuser can be moved along the optic axis to change the speckle size of the measured interference patterns, with best results achieved with a speckle size that covers around 3–8 detector pixels; Fig. 1(b) shows a typical diffraction pattern with a speckle size in this range. Each diffraction pattern comprises an average of 16 frames, each exposed for 200 μs and corrected by subtraction of a dark-field reference. The patterns were binned by 2, to 1024 \times 1024 pixels, resulting in a pixel size for our reconstructed images of 0.64 μm . A full ptychographic dataset is collected from the microscope by recording a series of between 20 and 400 of these diffraction patterns as the sample is laterally translated through a Fermat spiral pattern of scan positions (which prevents raster grid artifacts), with a 25 μm step between each position [14].

Reconstruction algorithm. The recorded diffraction data is fed into a version of the 3PIE algorithm [4] adapted for a near-field operation by replacing the final far-field (FFT) propagation from a sample to a detector with an angular spectrum

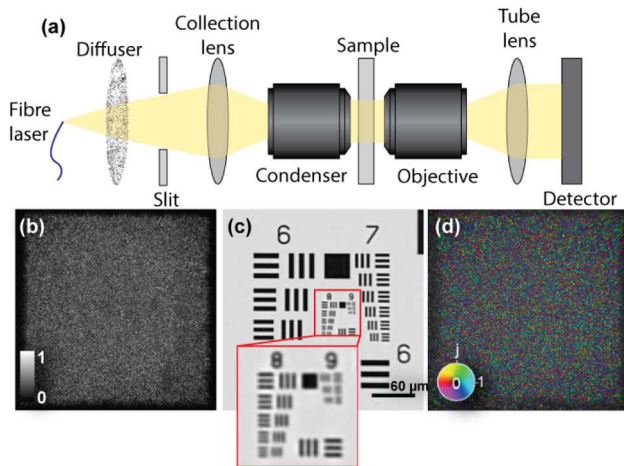


Fig. 1. (a) Experimental configuration. (b) Example near-field diffraction pattern captured by the detector. (c) Reconstructed modulus image of a resolution target with a zoomed-in view of groups 8 and 9, indicating a lateral resolution over 456.1 lp/mm. (d) Recovered illumination wavefront.

propagator. A MATLAB implementation of this modified 3PIE algorithm is available from [Code 1](#), Ref. [15], where several further modifications are also introduced:

1. Tikhonov regularization of the slice updates. This controls weakly constrained low spatial frequencies as iterations progress: without this the algorithm tends to introduce low spatial frequency artifacts [11,16].
2. Tapering of the update rate for each slice, so that upstream slices (nearest the detector) update more slowly than downstream slices. Without this the algorithm preferentially updates upstream slices, and features in downstream slices take a considerable number of iterations to emerge.
3. Additional probe modes. Interestingly, although coherence was not an issue with our fiber-coupled laser source, using two modes [17] to model the illumination wavefront greatly improves the convergence speed without detriment to the image quality.

We utilize a two-step reconstruction strategy for the results shown here. First, an accurate model of the illumination wavefront is recovered using 250 iterations of the modified 3PIE, with five slices evenly spaced through the sample volume. Then the number of slices is increased to any desired amount before running a further 250 iterations.

An example dataset and associated reconstruction parameters are available from [Dataset 1](#), Ref. [18].

Results. First, the lateral resolution of the system was assessed using a 1951 USAF resolution target, which resulted in the reconstructed image shown in Fig. 1(c) and the reconstructed illumination wavefront shown on a colorwheel scale in Fig. 1(d). The smallest set of bars in group 8 of the pattern are clearly resolved here, corresponding to a lateral resolution of $\delta_{lateral} = 1.1 \mu\text{m}$. The DoF in a ptychographic imaging system is generally defined by Eq. (1):

$$T = \frac{c(\delta_{lateral})^2}{\lambda} \quad (1)$$

where λ is the wavelength of the illumination and the constant c is variously reported as between 1 and 5.2 [19–21].

This suggests a DoF for the system in Fig. 1 of 1.8 – 9.3 μm . Conventional (non-multi-slice) ptychography results in image reconstructions showing considerable out-of-focus diffraction artifacts for samples beyond the upper end of this thickness and for sample thicknesses well beyond this limit multiple scattering causes convergence failure.

We next demonstrated the versatility of our method using three samples that show a range of phase variation and structure complexity: lily pollen, an algae colony, and a whole aphid.

The lily pollen grains were approximately 40 μm thick—exceeding the DoF of Eq. (1) by a factor of at least 4. The grains were stained and mounted on a standard microscope slide beneath a 200 mm coverslip. Following the data collection and reconstruction procedure as described, 43 slices spaced 0.95 μm apart were reconstructed from a set of 400 diffraction patterns. Figure 2 shows the recovered projected phase of the full sample volume on the left: this is obtained by summing the phases of the individual slices. Examples of four reconstructed slices are shown on the right, corresponding to the indicated positions within the sample volume (the most downstream plane of the sample is positioned at 0 μm). [Visualization 1](#) shows a movie of all 43 slices, and the sample volume is rendered in 3D in [Visualization 2](#). The multi-slice reconstruction allows us to identify structural detail within individual slices that is not apparent in the 2D projection, including the cell wall, tube nucleus, pollen wall, and aperture.

A second sample, a volvox colony 90 μm thick and mounted in the same way, produced the reconstruction shown in Fig. 3. The reconstruction comprises 41 slices, spaced 2.25 μm apart. To the left, the phases of all 41 slices are added to produce a single projection through the sample. The DoF is at least 10 times the DoF of the microscope objective, and the projection remains free from diffraction and multiple-scattering artifacts, leaving only blurring due to the missing wedge of low spatial frequencies. Examples of individual slices through the volvox are shown to the right at the indicated range of sample depths. A movie of the reconstruction can be viewed in [Visualization 3](#).

In a final test, we imaged an unstained, whole aphid sample with an approximate thickness of 140 μm , at least 14 times the DoF. The exoskeleton structure and soft tissue of this sample exhibit very different optical densities, which can be particularly challenging for conventional light microscopy: standard bright-field microscope images, taken with the same objective lens and an approximately matched condenser NA, are shown in the top row of Fig. 4 and clearly demonstrate the difficulty posed by background light and diffraction when attempting to clearly resolve features at different depths through this thick sample. (DoF for this bright-field setup was estimated at approximately 5 μm). The multi-slice reconstruction of 44 individual slices separated by 3 μm produced the zoomed-in phase images shown in the middle row of Fig. 4, with the bottom row showing the full field of view. The high-resolution visualization of both the internal and external structures of the aphid is made clear across a significant depth range here, well beyond the limits of the conventional microscope. Furthermore, the phase information obtained at different depths provides better contrast and richer structural detail. The complete reconstruction of all 44 slices is shown in [Visualization 4](#).

Data collection and reconstruction times are a potential drawback for multi-slice ptychography and are in general the most significant weakness in the ptychographic method. For the results shown in Figs. 2–4, 400 diffraction patterns were

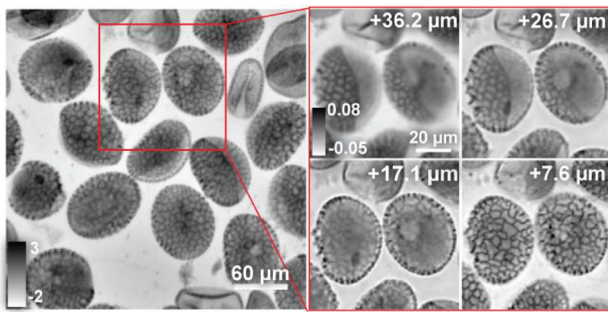


Fig. 2. Reconstructed phase images of liliun pollen grains, computationally sectioned using multi-slice ptychography. Left: pixel-wise product of all 43 reconstructed slice phases. Right: examples of individual slices at the indicated depths through the sample volume.

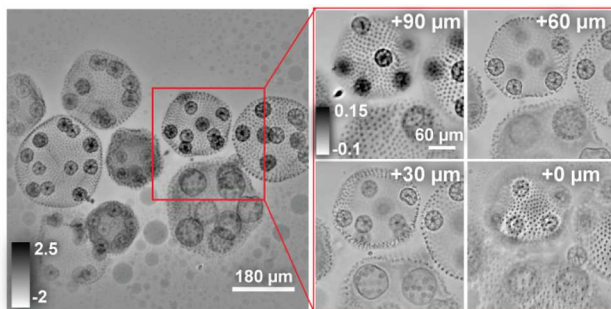


Fig. 3. Reconstructed phase images of a volvox, computationally sectioned using multi-slice ptychography. Left: pixel-wise product of all 41 reconstructed slices. Right: examples of individual slices at the indicated depths through the sample volume.

collected, taking, in total, around 600 s for data collection and 8283 s to run through the reconstruction. To reduce these times, we investigated the effect of collecting fewer diffraction patterns. Figure 5 displays the 33rd slice out of the 44 slices, showing the aphid embryo and reproductive organ, reconstructed using (a) 100, (b) 50, (c) 25, and (d) 16 diffraction patterns. The smaller datasets were created simply by discarding the outer parts of the spiral scan pattern while maintaining the same step size, and no pre-reconstructed illumination wavefront was used to seed these reconstructions. Both data collection and reconstruction times fall linearly with the number of diffraction patterns, so that the dataset containing 50 patterns took 75 s to collect and 496 s to reconstruct.

Notably, with 50–100 diffraction patterns (Figs. 5(a) and 5(b)), the aphid embryo's reproductive organ remains clearly visible, and lateral and axial resolutions are comparable to the reconstruction using 400 patterns. A further reduction to 25 diffraction patterns (Fig. 5(c)) results in significantly lower signal-to-noise ratio, obscuring fine details, but most features remain recognizable. When the number of total diffraction patterns is reduced to 16 (Fig. 5(d)), the reconstruction fails. Visualization 5 provides a comparison of reconstructions with reduced diffraction pattern number, further illustrating the decrease in phase contrast, especially in upstream slices, as the number of patterns is reduced.

Two further important experimental factors are key to achieving successful, high-quality phase images from our setup. Firstly,

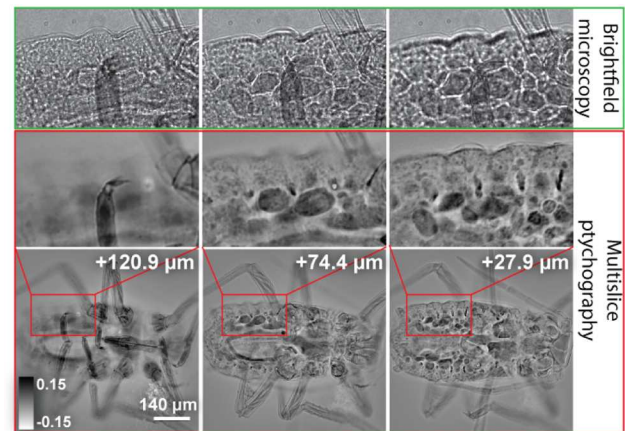


Fig. 4. Reconstructed slices of a whole aphid through the full sample volume. The red boxes show a zoomed-in view of the reproductive organs. A series of images taken using a compound light microscope at the same depth and cropped to the same region for comparison.

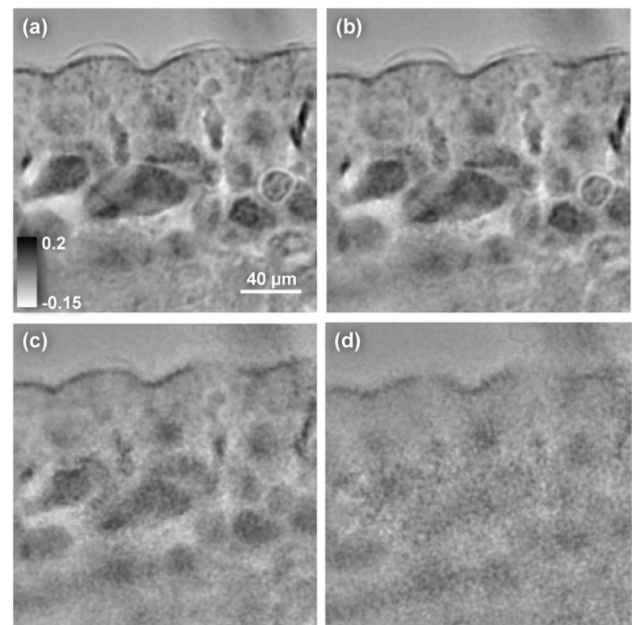


Fig. 5. Selected slice from multi-slice reconstructions of the aphid sample, using fewer diffraction patterns. (a) 100 diffraction patterns; (b) 50 diffraction patterns; (c) 25 diffraction patterns; (d) 16 diffraction patterns.

a diffuser with a fine speckle in the illumination path is crucial for achieving high resolution. Ideally, the speckles should be highly random and contain high spatial frequencies to fully utilize the illumination NA. This ensures rapid evolution of the illumination field along the propagation direction, which allows us to recover clean sample slices at minimal axial separation. Secondly, a small step size—close to the largest speckle size in the illumination—significantly improves the signal-to-noise ratio; however, if the step size is smaller than the average speckle size, the lack of diversity in the recorded data can lead to poor convergence or failure of the reconstruction.

In this Letter, we have showcased reconstruction results for computational sectioning of thick biological samples

via multi-slice near-field ptychography, incorporating speckle-modulated illumination on a standard microscope platform. We achieved an axial resolution below 10 μm over 40 computationally recovered slices at a lateral resolution of 1 μm . This allows a detailed visualization of the complex structures of biological samples across a significant depth. Notably, our near-field implementation of multi-slice ptychography requires significantly less data to cover a large field of view than do other methods [5,11]—typically fewer than 100 diffraction patterns. Furthermore, our method uses a simple and easily calibrated optical setup with a fixed optical path during data acquisition, which is adapted easily for different resolutions (both lateral and depth) through adjustment of the numerical aperture of the condenser and objective—[Visualization 6](#) shows a reconstruction of lily pollen grains using a 40 \times , 0.75 NA objective.

Limits on the maximum sample thickness, the number of slices that can be recovered, the optimal scan pattern, and the optimal illumination structure are currently under investigation: likely the breakdown of the multi-slice model will eventually limit the thickness that can be imaged at a given resolution, although improved models have been demonstrated and could be incorporated in this work [22].

Ultimately, this research paves the way for further development and applications, in particular through combination with tomography [23] for fully isotropic 3D volumetric microscopy of thick, strongly scattering samples.

Funding. Biotechnology and Biological Sciences Research Council (BB/X003221/1).

Disclosures. The authors declare no conflicts of interest.

Data availability. An example dataset underlying the results presented in this Letter is available in [Dataset 1](#), Ref. [18].

REFERENCES

1. T. Wang, S. Jiang, P. Song, *et al.*, *Biomed. Opt. Express* **14**, 489 (2023).
2. K. Lee, J. Jung, S. Lee, *et al.*, *ACS Photonics* **8**, 1307 (2021).
3. S. Jiang, J. Zhu, P. Song, *et al.*, *Lab. Chip* **20**, 1058 (2020).
4. A. M. Maiden, M. J. Humphry, and J. M. Rodenburg, *J. Opt. Soc. Am. A* **29**, 1606 (2012).
5. T. Godden, R. Suman, M. Humphry, *et al.*, *Opt. Express* **22**, 12513 (2014).
6. C. Guo, S. Jiang, L. Yang, *et al.*, *Biosens. Bioelectron.* **224**, 115049 (2023).
7. L. Tian and L. Waller, *Optica* **2**, 104 (2015).
8. A. Suzuki, S. Furutaku, K. Shimomura, *et al.*, *Phys. Rev. Lett.* **112**, 053903 (2014).
9. H. Öztürk, H. Yan, Y. He, *et al.*, *Optica* **5**, 601 (2018).
10. S. Gao, P. Wang, F. Zhang, *et al.*, *Nat. Commun.* **8**, 163 (2017).
11. S. Chowdhury, M. Chen, R. Eckert, *et al.*, *Optica* **6**, 1211 (2019).
12. R. Clare, M. Stockmar, M. Dierolf, *et al.*, *Opt. Express* **23**, 19728 (2015).
13. Z. Hu, Y. Zhang, P. Li, *et al.*, *Opt. Express* **31**, 15791 (2023).
14. X. Huang, H. Yan, R. Harder, *et al.*, *Opt. Express* **22**, 12634 (2014).
15. Z. Hu, Y. Zhang, and A. Maiden, "Modified 3PIE algorithm for near-field multi-slice ptychography," shef.data (2024), <https://doi.org/10.15131/shef.data.25773630.v1>.
16. Z. Chen, Y. Jiang, Y. Shao, *et al.*, *Science* **372**, 826 (2021).
17. P. Thibault and A. Menzel, *Nature* **494**, 68 (2013).
18. Z. Hu, Y. Zhang, and A. Maiden, "Dataset for near-field multi-slice ptychography," shef.data, 2024, <https://doi.org/10.15131/shef.data.25833298.v1>.
19. E. Tsai, I. Usov, A. Diaz, *et al.*, *Opt. Express* **24**, 29089 (2016).
20. M. Stockmar, M. Hubert, M. Dierolf, *et al.*, *Opt. Express* **23**, 12720 (2015).
21. M. Du, Z. Di, D. Gürsoy, *et al.*, *J. Appl. Crystallogr.* **54**, 386 (2021).
22. M. Chen, D. Ren, H. Liu, *et al.*, *Optica* **7**, 394 (2020).
23. P. Li and A. Maiden, *Sci. Rep.* **8**, 2049 (2018).